
1 **Holocene sea-level change on the central coast of Bohai Bay,** 2 **China**

3
4 Fu Wang^{1,2}, Yongqiang Zong³, Barbara Mauz^{4,5}, Jianfen Li^{1,2}, Jing Fang⁶, Lizhu Tian^{1,2},
5 Yongsheng Chen^{1,2}, Zhiwen Shang^{1,2}, Xingyu Jiang^{1,2}, Giorgio Spada⁷ and Daniele Melini⁸

6 ¹Tianjin Center, China Geological Survey (CGS), Tianjin, China

7 ²Key Laboratory of Coast Geo-Environment, China Geological Survey, CGS, Tianjin, China

8 ³Department of Earth Sciences, The University of Hong Kong, Hong Kong SAR, China

9 ⁴School of Environmental Sciences, University of Liverpool, Liverpool, UK

10 ⁵Department of Geography and Geology, University of Salzburg, Salzburg, Austria

11 ⁶School of Geography and Environmental Sciences, Tianjin Normal University, Tianjin, China

12 ⁷Department of Science, University of Urbino, Urbino, Italy

13 ⁸Istituto Nazionale di Geofisica e Vulcanologia, Roma, Italy

14 *Correspondence to: Fu Wang (wfu@cgs.cn)*

15
16 Abstract. To constrain models on global sea-level change regional proxy data on coastal change are
17 indispensable. Here, we reconstruct the Holocene sea-level history of the northernmost China Sea shelf. This
18 region is of great interest owing to its apparent far-field position during the late Quaternary, its broad shelf and
19 its enormous sediment load supplied by the Yellow River. This study generated 25 sea-level index points for
20 the central Bohai coastal plain through the study of 15 sediment cores and their sedimentary facies,
21 foraminiferal assemblages and radiocarbon dating the basal peat. The observational data were compared with
22 sea-level predictions obtained from global GIA models and with published sea-level data from Sunda shelf,
23 Tahiti and Barbados. Our observational data indicate a phase of rapid sea-level rise from c. -17 m to -4 m
24 between c. 10 ka and 5 ka with a peak rise of 6.4 mm/a during 8.7 ka to 7.5 ka and slower rise of 1.9 mm/a
25 during 7.5 ka to 5.3 ka followed by a phase of slow rise from 5 ka to 2 ka (~0.4 mm/a from -3.58 m of 5.3 ka
26 cal BP to -2.15 m of 2.3 ka cal BP). The comparison with the sea-level predictions for the study area and
27 the published sea-level data is insightful: in the early Holocene Bohai Bay's sea-level rise is dominated by a
28 combination of the eustatic and the water load components causing the levering of the broad shelf. In the mid-

29 late Holocene the rise is dominated by a combination of tectonic subsidence and fluvial sediment load which
30 masks the mid-Holocene highstand recorded elsewhere in the region.

31

32

33 **KEYWORDS:** Sea level; Holocene; Glacial Isostatic Adjustment; Ice Equivalent Sea Level; Bohai Bay

34 **1. Introduction**

35 The sea-level rise since the mid-19th century is one of the major challenges to humanity of the 21st century
36 (IPCC, 2014). The driving mechanisms of this rise are relatively well-known on a global scale, but on a regional
37 scale the mechanisms are modified by regional Holocene sea-level history, This history is a background signal
38 controlled by ice load and corresponding response of the the deformable Earth (Clark et al., 1978) and, in
39 addition, by regional parameters such as fluvial sediment supply and shelf geometry. In fact, the regional
40 response to sea-level changes may be very different from the global signal (Nicholls and Cazenave, 2010), and,
41 understanding regional costal environment is a rising demand of policy makers.

42 Here, we study the Holocene sea-level history of Bohai Sea, which is the northernmost part of China Sea (Fig.
43 1) and situated in the far-field of the former ice sheets. The area is of special interest because it receives a large
44 amount of fine-grained Yellow River sediment and because its shoreline is situated on the broad shelf of the
45 East China Sea (Fig. 1). During the Holocene sea-level rise the increasing water load in the west Pacific Ocean
46 basin should have lifted the Bohai Sea shelf and push the shoreline landward while the fluvial sediment input
47 should have pushed the shoreline seaward. The two processes may have peaked at different times and their
48 contrasting effect on shoreline migration may have varied accordingly. Beyond that, being situated in the far-
49 field, the shoreline should have migrated landward in response to the rising water level. The shelf effect and
50 the rising water level is well-described by sea-level physics and the associated glacio-isostatic adjustment (GIA)
51 models predict a sea-level elevated by up to 10 m height due to shelf levering (e.g. Milne and Mitrovica, 2008).
52 Indeed, a several meter sea-level highstand is predicted for the East China Sea coast during the mid-Holocene
53 (Bradley et al., 2016) but this high highstand seems to be an overestimate when compared to observational data

54 (Bradley et al., 2016) which indicate a minor Holocene highstand for East China Sea coast (Zong, 2004), and
55 no obvious Holocene highstand for delta area of Yangtze River (Xiong et al., 2020) and the Pearl River delta
56 (Xiong et al., 2018). From this the question arises, if the observational data are inaccurate, if the GIA model
57 parameters are too poorly constrained and how fluvial sediment supply influences the sea-level history.

58 In our study area, observational data were firstly obtained from chenier ridges (Wang, 1964). Subsequently, a
59 series of studies on marine transgression and lithostratigraphy provided the framework for understanding the
60 late Quaternary evolution of Bohai Bay (e.g., Zhao et al., 1979; Fig. S1) and, over time, over 130 Holocene
61 sea-level data, generated in the study area since the early 60ths, were recently compiled by Li et al. (2015; Fig.
62 S2; for details see supplement). However, because no correction for compaction was carried out, uncertainties
63 were poorly constrained and no screening took place by which unsuitable material (e.g., transported shell) is
64 rejected, the dataset requires further scrutiny and is not used in our study. Instead, we established new sea-level
65 data based on saltmarsh peat or peaty clay collected from drilling cores and compared with glacio-isostatic
66 adjustment (GIA) model predictions. The difference between model and observational datum should allow
67 inferring the non-GIA, hence fluvial, impact on the sea-level history. We show here that shelf effect and local
68 processes influence the regional sea-level history at different times.

69 **2. The study area**

70 The study area lies in a mid-latitude, temperate climate zone (Fig. 1a) on the north-western coast of the East
71 China Sea's wide shelf. Geologically, the Bohai Bay is a depression filled by several kilometre-thick
72 Cenozoic sediment sequences with the top 500 m ascribed to the Quaternary (Wang and Li, 1983). The long-
73 term tectonic subsidence has been estimated to about 1.3-2.0 mm/a at Tianjin City (Wang et al., 2003). The
74 Bay is a semi-enclosed marine environment, connected to the Pacific through a gap between the two
75 peninsulas, Liaodong Peninsulas and Shangdong Peninsulas and the Yellow Sea (Fig. 1b). Our study area is
76 the central coast of the Bay which lies between two deltaic plains, the Yellow River delta in the south and the
77 Luan River delta in the north (Fig. 1b). Several small rivers (e.g., Haihe and Duliujianhe, Fig. 1c) cut through
78 the coastal plain and enter the Bay. The coastal lowland is characterised not only by its low-lying nature,

79 (less than 10 m above sea level), but also by a series of chenier ridges situated south of the Haihe River and
80 buried oyster reefs situated north of the Haihe River (Fig. 1c; Li et al., 2007; Su et al., 2011; Wang et al.,
81 2011; Qin et al., 2017). Local reference tidal levels such as mean high waters (MHW) and highest high
82 waters (HHW) are 1.25 m and 2.30 m respectively, based on the four tidal stations on the coast of Bohai Bay
83 (Fig. 1c). During the Last Glacial Maximum the shoreline moved to the shelf break of the Yellow Sea, more
84 than 1000 km to the east and southeast of our study area (e.g., He, 2006). During the Holocene the sea
85 inundated the coastal area with the shoreline moving about 80 km inland (e.g., Wang et al., 2015).

86 **3 Methods**

87 **3.1 Sampling and elevation measurements**

88 To obtain sedimentary sequences for this study, we consulted previous studies (e.g. Cang *et al.*, 1979; Geng,
89 1981; Wang *et al.*, 1981; Wang, 1982; Yang and Chen, 1985; Zhang *et al.*, 1989; Zhao *et al.*, 1978; Xue et
90 al., 1993) to learn where in the bay marine deposits are dominant and where the landward limit of the last
91 marine transgression should occur. We then collected 15 cores along W-E transects from the modern
92 shoreline to 80 km inland (Fig. 1c), using a rotary drilling corer. Transect A, comprising 6 cores, stretches
93 from the modern shoreline 80 km inland and crosses the inferred Holocene transgression limit (Xue, 1993).
94 Transects B, C and D, comprising 9 cores, cross the transgression limit a little further south (Fig. 1c). The
95 surface elevations of the drilled cores were levelled to the National Yellow Sea 85 datum (or mean sea level,
96 MSL) using a GPS-RTK system with a precision of 3 cm. The GPS-RTK raw data were corrected and
97 processed to National Yellow Sea 85 datum system by the CORS system network available from the Hebei
98 Institute of Surveying and Mapping with National measurement qualification.

99 **3.2 Sediment and peat analyses**

100 In the laboratory, the sediment cores were opened, photographed and recorded for sedimentary characteristics
101 including grain size, colour, physical sedimentary structures, and content of organic material. To study the
102 degree of marine influence in the muddy sediment sequences, sub-samples were collected in 20 cm intervals.
103 These were analysed with respect to diatoms and foraminifera with a subsequent focus on the foraminifera

104 due to poor preservation of diatoms. The foraminifera of the >63 μ m fraction of 20 g dry sample were
105 counted (e.g., Wang et al., 1985) following studies on modern foraminifera (e.g. Li, 1985; Li et al., 2009).
106 Sediment description followed Shennan et al. (2015): where in the sediment sequences foraminifera first
107 appear and/or significantly increase (from zero or less than 10 to more than 50) is noted as transgressive
108 contact, while the sediment horizon where foraminifera disappear and/or decrease significantly are noted as
109 regressive contact. These changes are often associated with lithological changes, such as from salt-marsh
110 peaty sediment to estuarine sandy sediment or tidal muddy sediment across a transgressive contact, or vice
111 versa. In addition, peat material was analysed in terms of its foraminifera content so that salt-marsh peat can
112 be differentiated from freshwater peat.

113 **3.3 Analysis of compaction**

114 Because the Holocene marine deposits are mainly unconsolidated clayey silt with around 0.74% organic
115 matter (Wang et al. 2015) post-depositional auto-compaction (Brain et al., 2015) may have led to lowering of
116 the SLIP. According to Feng et al. (1999), the water content and compaction of marine sediments show
117 positive correlation with the down-core reduction of water content of the Holocene marine sediment being
118 about 10%. Based on these observations, we assumed the maximum lowering is about 10% of the total
119 thickness of the compressible sediment beneath each SLIP. Consequently, the total lowering for an affected
120 SLIP is 10% of the total thickness of the compressible sequence beneath the dated layer divided by the post-
121 depositional lapse time proportional to the past 9000 years (e.g. Xiong et al., 2018), i.e. since the marine
122 transgression in the study area.

123 **3.4 Radiocarbon analyses**

124 69 bulk organic sediment samples from salt-marsh peat were collected from drilling cores, and the peat or
125 plant subsamples obtained from these bulk sediments were chosen for AMS radiocarbon analysis at Beta
126 Analytic Inc. because these can give more reliable ages than shells for the SLIPs. The resulting raw
127 radiocarbon ages were converted to conventional ages after isotopic fractionation were corrected based on
128 $\delta^{13}\text{C}$ results. The conventional radiocarbon ages were calibrated to calendar years using the data set Intcal13

129 included in the software Calib Rev 7.0.2 for organic samples, peat and plant samples (Reimer, *et al.*, 2013).
130 Because Shang et al. (2018) reported age overestimation of 467 years for the bulk organic fraction of salt-
131 marsh peaty clay compared to the corresponding peat fraction, all the AMS ^{14}C ages between 4000 to 9000
132 BP obtained from salt-marsh samples were corrected by $Y=0.99X-466.5$ (Y is the corrected age, X is the age
133 obtained from the organic fractions; Shang et al., 2018) except one <600 years age from borehole Q7 (Table
134 1).

135 3.5 Sea-level index points (SLIPs)

136 To develop SLIPs, salt-marsh peaty clay layers were used. To convert the dated peat layers into a SLIP, the
137 modern analogue approach was used by measuring the elevation of the modern open tidal flat (Fig. 2) and
138 sampling its surface for their foraminiferal content. Following the studies of the modern foraminifera
139 assemblage (Li, 2009) *Ammonia beccarii* typically occurs in the upper part of an intertidal zone and
140 *Elphidium simplex* in the lower intertidal zone. The zonation of the modern foraminifera assemblage was
141 then used to identify the indicative meaning of the salt-marsh peat layers: the paleo-mean sea level is the
142 midpoint between high water of spring tides (HHW:+2.3 m) and mean high waters (MHW:+1.25 m) which is
143 1.78 m with ± 0.53 m uncertainty (Wang et al., 2012, 2013; Li et al., 2015). For each dated salt-marsh peat
144 layer the indicative meaning and range, the total amount of possible lowering in elevation due to sediment
145 compaction and the reconstructed elevation of palaeo-MSL are listed in Table 1.

146 3.6 GIA modelling

147 The time-evolution of sea level was obtained using the open source program SELEN (Spada and Stocchi,
148 2007) to solve the "Sea Level Equation" (SLE) in the standard form proposed in the seminal work of Farrell
149 and Clark (1976). In its most recent development, SELEN (version 4) solves a generalized SLE that accounts
150 for the horizontal migration of the shoreline in response to sea-level rise, for the transition from grounded to
151 floating ice and for Earth's rotational feedback on sea level (Spada and Melini, 2019). The programme
152 combines the two basic elements of GIA modelling (Earth's rheological profile and ice melting history since
153 the Last Glacial Maximum) assuming a Maxwell viscoelastic incompressible rheology. The GIA models
154 adopted are ICE-5G(VM2) (Peltier et al., 2004), ICE-6G(VM5a) (Peltier et al., 2012), both available on the
155 home page of WR Peltier, and the one developed by Kurt Lambeck and colleagues (National Australian

156 University, denoted as ANU hereafter; Nakada and Lambeck, 1987, Lambeck et al., 2003) provided to us by
157 A Purcell (pers. com. 2016). Table S1 summarises the values used for each model. The palaeo-topography
158 has been solved iteratively, using the present-day global relief given by model ETOPO1 (Amante and Eakins,
159 2009). All the fields have been expanded to harmonic degree 512, on an equal-area icosahedron-based grid
160 (Tegmark, 1996) with a uniform resolution of ~20 km. The rotational effect on sea-level change has been
161 taken into account by adopting the “revised rotational theory” (Mitrovica and Wahr, 2011).

162 **4. Results**

163 4.1 Lithostratigraphy and facies

164 Lithostratigraphically, the cores show a succession of terrigenous (including fresh-water swamp, river
165 channel, flood plain), salt marsh and marine sediments (Table S2) with a clear W-E trend from terrestrial to
166 marine dominance of deposits (Fig. 3-6). The around 80 km long transect A shows this trend: close to the
167 modern shoreline pre-Holocene terrigenous sediments are overlain by basal peat including salt-marsh peat or
168 peaty clay. Further inland these are replaced by fresh-water peat overlain by salt marsh and intertidal
169 sediments and, above, by terrigenous sediments. The cores DC01, CZ01 and CZ02 are composed of fluvial
170 sediments only, roughly confirming the Holocene maximum transgression inferred by Xue (1993). Multiple
171 shifts between salt marsh, marine and fluvial deposits are noticeable in cores QX02, QX03, CZ61 which
172 originate from the central part of the study area.

173 Marsh deposits are either a blackish and thin freshwater peat mostly interbedded in yellowish fluvial
174 sediments or a yellowish-brown salt-marsh peat bearing intertidal foraminifera (Table 1). Their lower
175 boundaries are usually sharp, and their upper boundaries are mostly diffused or the salt-marsh peat changes
176 gradually into dark grey intertidal sediments. Salt-marsh peat is intercalated in marine sediment sequences
177 (i.e. QX01, QX02, CZ61, CZ85, CZ66 and CZ03, Fig. 3-6), particularly at sites that are close to the
178 Holocene maximum transgression limit.

179 4.2 Foraminifera data

180 Foraminifera were identified in all cores except CZ01, CZ02 and DC01 which originate from the landward
181 site of the maximum transgression limit. As the Fig. 4 and 6 show that, foraminifera start to appear at 11.2 m
182 depth, which is dated to about 7.85 ka cal BP in QX01. Abundance of fossil foraminifera changes from about

183 404 – 772 individuals per samples at depths from 11.2 m to 10.8 m, 68 – 338 specimens from 9.4 m to 8.8 m,
184 and 103 – 3456 counts from 8.2 m to 7.6 m. The assemblages reach maximum abundance at 6.6 m depth
185 which is dated to between 5.29 and 5.23 ka cal BP, with over 30,000 individuals per sample, before
186 disappearing at 5.6 m. Dominant species change from *Nonion glabrum* in 11.2 – 7.4 m to *Ammonia beccarii*
187 vars. in 7.4 – 6.4 m. This change represents a change from a salt marsh to a lagoon. In QX02, the pattern of
188 foraminifera distributions is very similar. Low numbers of foraminifera, mostly *Nonion glabrum*, start to
189 appear at about 10.1 m (-6.53 m of sea level), as dated to between 7.87 and 7.49 ka cal BP. The abundance
190 reaches its highest at 6.7 m (-3.13 m of sea level), and the assemblages were dominated by *Ammonia beccarii*
191 vars. Foraminifera disappears sometime between 5.72 and 3.52 ka cal BP. In all seaward drilling core, CZ03,
192 CZ80, CZ85, CZ66, CZ87, CZ61, CZ65, ZW15 and Q7, the pattern of foraminifer's distributions are very
193 similar as QX01 and QX02 (Fig. 4). The foraminifera start to appear in low numbers in the layer just above
194 the basal peaty clay. This first appearance is in ca. 17-8 m depth dated to 9-7 ka cal BP. Above this depth the
195 count increases from ~100 to ~3000 foraminifera per sample at ca 8-7 m depth. The maximum count
196 with >30,000 individuals per sample is reached at -6-5 m dated to around 5 ka cal BP. Foraminifera
197 disappear in these cores sometime between 5.7 ka cal BP and 3.5 ka cal BP. The foraminifera assemblage is
198 composed of few species only, hence not rich and first dominated by *Nonion glabrum* in 17-7 m depth and
199 then dominated by *Ammonia beccarii* vars. in 7-6 m depth. Other species found are *Quinqueloculina*
200 *akneriana rotunda* and *Protelphidium tuberculatum* (Figs. 4 and 6).

201 4.3 Modern analogue and indicative meaning and range

202 The data obtained from the modern analogue shows that the tidal flat can be divided into two sub-
203 environments: intertidal with bioturbation (worm hole developed in tidal surface) and supratidal with salt-
204 marsh vegetation (Fig. 2). Within the supratidal and salt-marsh zones, the foraminiferal assemblages are
205 dominated by *Ammonia beccarii* covering an elevation range from +1.42 m to +2.00 m, including the +1.79m
206 boundary of salt marsh with plants. At sites below these elevations, i.e. intertidal with bioturbation (Fig. 2),
207 the foraminiferal assemblages are dominated by *Elphidium simplex*, *Ammonia beccarii* and *Pseudogyroidina*
208 *Sinensis*. This foraminiferal zone covers an elevation ranging from 1.42 m to modern MSL.

209 Besides occasional *A. beccarii* there are few living foraminifera in the salt marsh above the MHW. The
210 abundance is either biased towards *Ammonia beccarii* or it is relatively small. The latter is most probably due
211 to the area being situated above the MHW and, hence, subject to evaporation during low tide, with the
212 consequence of a relatively high and highly variable salt content of the pore water in the intertidal zone. The
213 modern analogue samples confirm the bias towards salt-tolerant species (Fig. 2, Table 1). The spatial
214 distribution of the ages confirms the E-W trend of the Holocene transgression where the oldest age is close to
215 the modern shoreline and the youngest age is close to the maximum transgression limit.

216 4.4 Sea-Level Index Points

217 In total 25 sea-level index points were established from the dated basal salt-marsh peat using the information
218 obtained from the modern analogue. In Core Q7, at the most seaward location in the study area, the basal
219 SLIP is dated to ~9700 cal BP (Table 1), marking the onset of marine inundation of the study area. The
220 overlying marine sequence is capped by a thick layer of shelly gravels at 1.30 m depth and the associated
221 SLIP is dated to 540 cal BP. This marks the upper end of the marine sequence as foraminifera start to
222 disappear alongside a change from intertidal to supratidal environmental conditions. The cores ZW15, QX02,
223 QX03, QX01 show the same sequence as Q7 and provide 6 SLIPs. 19 SLIPs were collected from other cores
224 (Table 1).

225 3. Discussion

226 5.1 Quality of SLIP data

227 Owing to elevated and variable salinity of the coastal water samples from both cores and modern tidal flat are
228 characterised by low microfauna diversity and low number of foraminifera species. This precludes the use of
229 transfer function statistics and compels analysis based on direct comparison with the modern environment.
230 We have solved this analytical problem by establishing SLIPs exclusively from basal salt-marsh peat in
231 transgressive contact and by correcting the data for compaction. This analytical rigor allowed generating
232 more accurate and more precise SLIP data than those reported by Li et al. (2015) because these earlier SLIP

233 data are characterised by relatively poor chronological and elevation control (for details see supplement).
234 Notwithstanding SLIP improvement in terms of accuracy and precision, fluctuation of the data exist that can
235 exceed 1 m (e.g. at 3.9 ka and at 5.2 ka, Fig. 7). Although hard to prove due to lack of data, we believe that
236 these fluctuations are caused by groundwater extraction which lowers the surface in places.

237 **5.2 The observed Holocene sea-level rise**

238 The SLIPs established indicate two phases of sea-level rise during the Holocene. The first phase occurred in
239 the early Holocene until ~6.5 ka when the sea level rose from -17 m to -4 m. The second phase occurred from
240 ~6.5 ka to 2 ka when the sea level rose from -4 m to -2 m. The oldest Holocene shoreline in Bohai Bay is,
241 situated at -17.2 m at ~9.7 ka cal BP, similar to Tian et al. (2017) who indicate ~-20 m at 9.4 ka cal BP based
242 on seismic units and drilling cores. Between around 8.8 ka and 7.5 ka cal BP the sea level rose rapidly from -
243 15.4 m to -7.0 m at a rate of ca 6.4 mm/a. Then, from 7.5 ka to 5.2 ka cal BP the relative sea level rose to -3.6
244 m at an average rate of 1.9 mm/a and to -1.2 m until 3.8 ka cal BP, before falling to -2.1 m at 2.3 ka cal BP
245 with an average rising rate of ca. 0.4mm/a from 5.2 to 2.3 ka cal BP. The final phase from 2 ka to today is
246 constrained by only one SLLP from core Q7 dated to 540 cal BP at ~0.5 m (Table 1). Lithostratigraphic data
247 (Shang et al., 2016) suggest that surface of the intertidal sediment body remained very close to zero m from
248 the landward limit of the marine transgression to about 2 km inland from the present shoreline. Further
249 inland, in borehole ZW15 the surface elevation of the same intertidal sediment body is ~3.0 m lower than in
250 core Q7 (Figs. 3 and 4) suggesting a rise of sea level in Bohai Bay in the last 1000 years.

251 **5.3 Observed and predicted Holocene sea level**

252 We compare our observational data with GIA models employed in this study and with Bradley et al. (2016;
253 henceforth denoted as BRAD; see also Table S1) who examined several ice-melting scenarios together with a
254 range of Earth-model parameters, and validated model outputs using published SLIP data from East China
255 Sea coast including Bohai Bay.

256 Figure 7a displays observational data and sea-level predictions generated in this study. It shows that none of
257 GIA models approximates the observations. The difference ranges between around 14 m at 9 ka and 3 m at

258 2.5 ka. Bohai Bay's oldest Holocene shoreline (~9.7 ka cal BP) is at -17.2 m (observed), at ca - 35 m (ANU)
259 or at ca -10 m (ICE-X). The BRAD model predicts this shoreline to be at ~-20 m at 10 ka. Our observed
260 shoreline elevation is similar to Sunda Shelf (ca -15 m; Hanebuth et al., 2011) but different to the islands of
261 Tahiti (ca -28 m; Bard et al., 2010) and Barbados (ca -25 m; Peltier and Fairbanks, 2006). There are two
262 ways to interpret this: (i) the age of the lowermost SLIP in core Q7 is overestimated due to old carbon
263 contamination of the dating material or, (ii) the relatively shallow shoreline position in our study area is a
264 deviation from eustasy due to levering of the broad continental shelf in response to ocean load (e.g., Milne
265 and Mitrovica, 2008). The similarity to the Sunda Shelf and absence of contamination elsewhere in the
266 sediment cores suggests indeed that the broad-shelf effect (East China Sea shelf; Fig. 1) causes the shallow
267 shoreline position. More SLIP data are needed to provide unequivocal evidence for it.

268 While SLIP data suggest a rising rate of ~0.4 cm/a during the early Holocene, the GIA models indicate ~0.5
269 cm/a (ICE-X) and ~0.9 cm/a (ANU). The ICE-X models approximate the observed early Holocene rising rate
270 but the timing of this rise is offset by about 2000 years. In the ANU model the early Holocene sea level rises
271 almost twice as fast as the observed one with an offset of ~500 years. Thus, the observed early Holocene sea
272 level rises slower than the modelled sea level. For the mid-late Holocene SLIP data suggest ~0.04 cm/a rising
273 rate while the GIA models indicate a falling sea level. Predictions obtained from ICE-5G and ICE-6G are
274 generally relatively similar but deviate from each other in the timing of the mid-Holocene sea-level
275 highstand. The GIA models, including BRAD, show the highstand (4.6 m -3.4 m; 0.5 m) at 7-6 ka while the
276 SLIP data remain below modern sea level until 2 ka. The misfit between observed and predicted sea level rise
277 is in the coastal zone south of Bohai Bay much smaller than in our study area (Fig. S3). This should reflect
278 the geological structure of the area: our study area belongs to the North China Plain Subsidence Basin (Wang
279 and Li, 1983), while the south of Bohai Bay lies on the edge of Shandong Upland (Fig.1b). Thus, the most -
280 likely explanation for the Bohai Bay misfit is subsidence of the coastal plain. Subsidence is a non-GIA
281 component and should become evident through the residuals (i.e. the difference between observation and
282 prediction per unit of time; Fig. 7b). Indeed, we identify linearity of residuals for the period 7-0 ka,
283 suggesting that subsidence dominates the local sea-level signal after the rise of the eustatic sea level has

284 slowed down. A subsidence rate of 1.25 mm/a is estimated from the residuals, similar to Wang et al. (2003)
285 who deduced a rate of ~1.5 mm/a from the 400-500 m thick Quaternary sequence in the bay. It is possible
286 that fluvial sediment supply enhanced the subsidence rate in the Holocene. The Yellow River's annual
287 discharge into Bohai Bay is estimated to 0.2 Gt until 740AD rising to 1.2 Gt until around 1800 when
288 widespread farming on the loess plateau started increasing the river's sediment load (Best, 2019). Thus, the
289 sea-level rise in Bohai Bay is in the early Holocene dominated by the eustatic sea-level rise and GIA effects
290 associated with the broad shelf from Bohai Sea to East China Sea, while in the mid-late Holocene it is
291 dominated by a combination of tectonic subsidence and fluvial sediment load.

292 **4. Conclusions**

293 Using advanced methods for field survey and identification of accurate and precise sea-level markers, we
294 have established a new Holocene sea-level history for central Bohai Bay. Our new data are not only different
295 to previously published data in that they do not show the expected mid-Holocene sea level highstand, but
296 they are also different to global GIA models. We see a possible broad-shelf effect elevating the shoreline by
297 several meters in comparison to the tropical islands of Tahiti and Barbados and we see local processes
298 controlling shoreline migration and coast evolution as soon as ice melting ceased. This indicates that more
299 emphasis should be placed on regional coast and sea-level change modelling under a global sea-level rising
300 future as the local government need more specific and effective advice to deal with coastal flooding.

301 **5. ACKNOWLEDGMENTS**

302 We thank one anonymous reviewer and Sarah Bradley for constructive suggestions on the manuscript. This
303 work was supported by the China Geological Survey, CGS (DD20189506) and National Natural Science
304 Foundation of China (Grant no. 41476074, 41806109, 41972196). The authors acknowledge PALSEA, a
305 working group of the International Union for Quaternary Sciences (INQUA) and Past Global Changes
306 (PAGES), which in turn received support from the Swiss Academy of Sciences and the Chinese Academy of
307 Science.

308 **References**

- 309 Amante, C. and Eakins, B.: ETOPO1 Arc-Minute Global Relief Model: Procedures, Data Source and
310 Analysis. Tech. rep, DOI: 10.7289/V5C8276M, 2009.
- 311 Bard, E., Hamelin, B. and Delanghe-Sabatier, D.: Deglacial meltwater pulse 1B and Younger Dryas sea
312 levels revisited with boreholes at Tahiti. *Science*, 327, 1235–1237. DOI: 10.1126/science.1180557, 2010.
- 313 Best, J.: Anthropogenic stresses on the world’s big rivers. *Nature Geoscience*, 12, 7–21.
314 Doi:10.1038/s41561-018-0262-x, 2019.
- 315 Bradley, S.L., Milne, G.A., Horton, B.P., Zong, Y.Q.: Modelling sea level data from China and Malay-
316 Thailand to estimate Holocene ice-volume equivalent sea level change. *Quaternary Science Reviews*, 137,
317 54–68. DOI: 10.1016/j.quascirev.2016.02.002, 2016.
- 318 Brain, M.J. Chapter 30 Compaction. In: Shennan, I., Long, A.J., Horton, B.P. (Eds.): *Handbook of Sea-level*
319 *Research*. John Wiley & Sons Ltd. Chichester, UK, 2015.
- 320 Cang, S.X., Zhao, S.L., Zhang, H.C., Huang, Q.F.: Middle Pleistocene paleoecology, paleoclimatology and
321 paleogeography of the western coast of Bohai Gulf. *Acta Palaeontologica Sinica* 18(6): 579–591. DOI:
322 10.19800/j.cnki.aps.1979.06.006, 1979 (in Chinese with English abstract).
- 323 Farrell, W. and Clark, J.: On postglacial sea-level. *Geophys. J. Roy. Astr. S.*, 46, 647–667. DOI:
324 10.1111/j.1365-246X.1976.tb01252.x, 1976
- 325 Feng, X.L., Lin, L., Zhuang, Z.Y, Pan, S.C.: The relationship between geotechnical parameters and
326 sedimentary environment of soil layers since Holocene in modern Huanghe subaqueous Delta. *Coastal*
327 *Engineering*, 18, 4, 1–7. DOI: CNKI:SUN:HAGC.0.1999-04-000, 1999 (in Chinese with English abstract).
- 328 Geng, X.S.: Marine transgressions and regressions in east China since late Pleistocene Epoch. *Acta*
329 *Oceanologica Sinica*, 3(1), 114–130.
330 http://www.hyxb.org.cn/aos/ch/reader/create_pdf.aspx?file_no=19810110&flag=&journal_id=aos&year_id
331 =1981, 1981 (in Chinese with English abstract).

- 332 Hanebuth, T.J.J., Voris, H.K., Yokoyama, Y., Saito, Y., Okuno, J.I.: Formation and fate of sedimentary
333 depocentres on Southeast Asia's Sunda Shelf over the past sea-level cycle and biogeographic implications.
334 *Earth-Science Reviews*, 104(1–3), 92–110. <https://doi.org/10.1016/j.earscirev.2010.09.006>, 2011.
- 335 He, Q.X.(Eds.): *Marine Sedimentary Geology of China*. Beijing: China Ocean Press: 464–466, 2006 (in
336 Chinese).
- 337 IPCC: *Climate Change 2014: Synthesis Report. Contribution of Working Groups I, II and III to the Fifth*
338 *Assessment Report of the Intergovernmental Panel on Climate Change [Core Writing Team, R.K. Pachauri*
339 *and L.A. Meyer (eds.)]*. IPCC, Geneva, Switzerland, 151 pp. <https://www.ipcc.ch/report/ar5/syr/>, 2014.
- 340 Lambeck, K., Purcell, A., Johnston, P., Nakada, M., Yokoyama, Y.: Water-load definition in the glacio-
341 hydro-isostatic sea-level equation. *Quaternary Science Reviews*, 137, 54–68. DOI: 10.1016/s0277-
342 3791(02)00142–7, 2003.
- 343 Li, J.F.; Kang, H.; Wang, H.; Pei, Y.D.; Modern geological action and discussion of influence factors on the
344 west coast of Bohai Bay, China. *Geological Survey and Research*, 30(4), 295–301.
345 <http://www.tianjin.cgs.gov.cn/dzdcyyj/qkxz/20074/200801/P020160920812081540884.pdf>, 2007 (in
346 Chinese with English abstract).
- 347 Li, J., Pei, Y., Wang, F., Wang, H.: Distribution and environmental significance of living foraminiferal
348 assemblages and taphocoenose in Tianjin intertidal zone, the west coast of Bohai Bay. *Marine geology &*
349 *Quaternary geology*, 29(3), 9–21. DOI: CNKI:SUN:HYDZ.0.2009-03-004, 2009. (in Chinese with English
350 abstract).
- 351 Li, J., Shang, Z., Wang, F., Chen, Y., Tian, L., Jiang, X., Wang, H.: Holocene sea level change on the west
352 coast of the Bohai Bay. *Quaternary Sciences*, 35(2), 243–264. DOI: 10.11928/j.issn.1001-
353 7410.2015.02.01, 2015 (in Chinese with English abstract).
- 354 Li, S.L.: Distribution of the foraminiferal thanatocoenosis of PEARL River estuary. *Marine geology &*
355 *Quaternary Geology*, 5(2), 83–101. DOI: 10.16562/j.cnki.0256-1492.1985.02.009, 1985 (in Chinese with
356 English abstract).

- 357 Milne, G.A. and Mitrovica J.X.: Searching for eustasy in deglacial sea-level histories. *Quaternary Science*
358 *Reviews*, 27, 2292–2302. DOI: 10.1016/j.quascirev.2008.08.018, 2008. Mitrovica, J. and Wahr, J.: Ice Age
359 Earth Rotation. *Annual Review of Earth and Planetary Sciences*, 39, 577–616. DOI: 10.1146/annurev-
360 earth-040610-133404, 2011.
- 361 Nakada, M. and Lambeck, K.: Glacial rebound and relative sea-level variations: a new appraisal.
362 *Geophysical Journal International*, 90, 1, 171–224. DOI: 10.1111/j.1365-246X.1987.tb00680.x, 1987.
- 363 Nicholls, R.J. and Cazenave A.: Sea-level rise and its impact on coastal zones. *Science*, 328, 1517–1520.
364 DOI: 10.1126/science.1185782, 2010.
- 365 Peltier, W.R.: Global glacial isostasy and the surface of the ice-age Earth: the ICE-5G (VM2) Model and
366 GRACE, *Annu. Rev. Earth Pl. Sc.*, 32, 111–149.
367 <https://doi.org/10.1146/annurev.earth.32.082503.144359>, 2004.
- 368 Peltier, W.R., Drummond, R., and Roy, K.: Comment on Ocean mass from GRACE and glacial isostatic
369 adjustment by DP Chambers et al., *J. Geophys. Res.-Sol. Ea.*, 117, B11403.
370 <https://doi.org/10.1029/2011JB008967>, 2012.
- 371 Peltier, W.R., and Fairbanks, R.G.: Global glacial ice volume and Last Glacial Maximum duration from an
372 extended Barbados sea level record, *Quat. Sci. Rev.*, 25(23), 3322–3337. DOI:
373 10.1016/j.quascirev.2006.04.010, 2006.
- 374 Qin, L., Shang, Z.W., Li, Y., Li, J.F.: Temporal and spatial distribution of the oyster reef in Biaokou to
375 Zengkouhe area; *Geological Survey and Research*, 40(4), 306–310.
376 <http://www.tianjin.cgs.gov.cn/dzdcyyj/qkxz/20174/201802/P020180202566954723921.pdf>, 2017 (in
377 Chinese with English abstract).
- 378 Reimer, P.J., Bard, E., Bayliss, A., Beck, J.W., Blackwell, P.G., Ramsey, C.B., Buck, C.E., Cheng, H.,
379 Edwards, R.L., Friedrich, M., Grootes, P.M., Guilderson, T.P., Haflidason, H., Hajdas, I., Hatté, C.,
380 Heaton, T.J., Hogg, A.G., Hughen, K.A., Kaiser, K.F., Kromer, B., Manning, S.W., Niu, M., Reimer,
381 R.W., Richards, D.A., Scott, E.M., Southon, J.R., Turney, C.S.M., van der Plicht, J.: *IntCal13 and*

- 382 MARINE13 radiocarbon age calibration curves 0–50000 years cal BP. *Radiocarbon*, 55(4), 1869–1887.
383 doi: 10.2458/azu_js_rc.55.16947Bronk Ramsey C and Lee S (2013), 2013.
- 384 Shang, Z.W., Wang, F., Li, J.F., Marshall, W.A., Chen, Y.S., Jiang, X.Y., Tian, L.Z., Wang, H.: New
385 residence times of the Holocene reworked shells on the west coast of Bohai Bay, China. *Journal of Asian*
386 *Earth Sciences*, 115, 492–506. DOI: 10.1016/j.jseaes.2015.10.008, 2016.
- 387 Shang, Z.W., Wang, F., Fang J., Li, J.F., Chen, Y.S., Jiang, X.Y., Tian, L.Z., Wang, H.: Radiocarbon ages of
388 different fractions of peat on coastal lowland of Bohai Bay: marine influence? *Journal of Oceanology and*
389 *Limnology*, <https://doi.org/10.1007/s00343-019-7091-7>, 2018.
- 390 Shennan, I., Long, A.J. and Horton, B.P.(Eds.): *Handbook of sea-level research*. Published by John Wiley &
391 Sons, Ltd., 2015.
- 392 Spada, G. and Stocchi, P.: SELEN: a Fortran 90 program for solving the “Sea Level Equation”, *Comput.*
393 *Geosci.*, 33, 538–562. DOI: 10.1016/j.cageo.2006.08.006, 2007.
- 394 Spada, G. and Melini, D.: SELEN4 (SELEN version 4.0): a Fortran program for solving the gravitationally
395 and topographically self-consistent sea-level equation in glacial isostatic adjustment modelling.
396 *Geoscientific Model Development*, 12, 5055–5075. DOI: 10.5194/gmd-12-5055-2019, 2019
- 397 Su, S.W., Shang, Z.W., Wang, F., Wang, H.: Holocene Chenier: spatial and temporal distribution and sea
398 level indicators in Bohai Bay. *Geological Bulletin of China*, 30(9), 1382–1395. DOI: 10.1007/s11589-011-
399 0776-4, 2011(in Chinese with English abstract).
- 400 Tian, L.Z., Chen, Y.P., Jiang, X.Y., Wang, F., Pei, Y.D., Chen, Y.S., Shang, Z.W., Li, J.F., Li, Y., Wang, H.:
401 Post-glacial sequence and sedimentation in the western Bohai Sea, China. *Marine Geology*, 388m 12–24.
402 <http://dx.doi.org/10.1016/j.margeo.2017.04.006>, 2017.
- 403 Tegmark, M.: An icosahedron-based method for pixelizing the celestial sphere, *Astrophys. J.*, 470, L81–L85,
404 <https://doi.org/10.1086/310310>, 1996.
- 405 Wang, F., Li, J.F., Chen, Y.S., Fang, J., Zong, Y.Q., Shang, Z.W., Wang H.: The record of mid-Holocene
406 maximum landward marine transgression in the west coast of Bohai Bay, China. *Marine Geology*, 359,
407 89–95. DOI: 10.1016/j.margeo.2014.11.013, 2015.

- 408 Wang, H., Chen, Y.S., Tian, L.Z., Li, J.F., Pei, Y.D., Wang, F., Shang, Z.W., Fan, C.F., Jiang, X.Y., Su,
409 S.W., Wang, H.: Holocene cheniers and oyster reefs in Bohai Bay: palaeoclimate and sea level changes.
410 Geological Bulletin of China, 30(9), 1405–1411. DOI: 10.1007/s11589-011-0776-4, 2011(in Chinese with
411 English abstract).
- 412 Wang, P.X., Min, Q.B. and Bian, Y.H.: Distributions of foraminifera and ostracoda in bottom sediments of
413 the northwestern part of the South Huanghai (Yellow) Sea and its geological significance. In: Wang, P.
414 (Eds.), Marine Micropaleontology of China. China Ocean Press, Beijing, pp. 93–114, 1985 (in Chinese
415 with English abstract).
- 416 Wang, P.X., Min, Q.B., Bian, Y.H., Cheng, X.R.: Strata of quaternary transgressions in east China: a
417 preliminary study. Acta Geologica Sinica, 1, 1–13. DOI: 10.1007/BF01077538, 1981 (in Chinese with
418 English abstract).
- 419 Wang, Q. and Li F.L.: The changes of marine-continental conditions in the west coast of the Bohai Gulf
420 during Quaternary. Marine Geology & Quaternary Geology, 4, 83–89. DOI: 10.16562/j.cnki.0256-
421 1492.1983.04.013, 1983 (in Chinese with English abstract).
- 422 Wang, R.B., Zhou, W., Li, F.L., Wang, H., Yang, G.Y., Yao, Z.J., Kuang, S.J.: Tectonic subsidence and
423 prospect of ground subsidence control in Tianjin area. Hydrogeology & Engineering Geology, 5, 12–17.
424 DOI: 10.1007/BF02873153, 2003 (in Chinese with English abstract).
- 425 Wang, Y.: The shell coast ridges and the old coastlines of the west coast of the Bohai Bay. Bulletin of
426 Nanjing University (Edition of Natural Sciences), 8(3), 424–440. DOI: CNKI:SUN:NJDZ.0.1964-03-007,
427 1964 (with three plates) (in Chinese with English abstract).
- 428 Wang, Y.M.: A preliminary study on the Holocene transgression on the coastal plain along the north-western
429 Bohai Bay. Geographical Research, 1(2), 59–69. DOI: 10.11821/yj1982020007, 1982 (in Chinese with
430 English abstract).
- 431 Wang, Z., Zhuang, C., Staito, Y., Chen, J., Zhan, Q., Wang, X.: Early mid-Holocene sea-level change and
432 coastal environmental response on the southern Yangtze delta plain, China: implications for the rise of
433 Neolithic culture. Quaternary Science Reviews, 35, 51–62. DOI: 10.1016/j.quascirev.2012.01.005, 2012.

- 434 Wang, Z., Jones, B.G., Chen, T., Zhao, B., Zhan, Q.: A raised OIS3 sea level recorded in coastal sediments,
435 southern Changjiang delta plain, China. *Quaternary Research*, 79, 424–438. DOI:
436 10.1016/j.yqres.2013.03.002, 2013.
- 437 Xiong, H., Zong, Y., Qian, P., Huang, G., Fu, S.: Holocene sea-level history of the northern coast of South
438 China Sea. *Quaternary Science Reviews* 194, 12–26. <https://doi.org/10.1016/j.quascirev.2018.06.022>,
439 2018.
- 440 Xiong, H., Zong, Y., Li, T., Long, T., Huang, G., Fu, S.: Coastal GIA processes revealed by the early to
441 middle Holocene sea-level history of east China. *Quaternary Science Reviews*, 233, 106249. DOI:
442 10.1016/j.quascirev.2020.106249, 2020.
- 443 Xue, C.T.: Historical changes in the Yellow River delta, China. *Marine Geology* 113, 321–329. DOI :
444 10.1016/0025-3227(93)90025-Q, 1993.
- 445 Yang, H.R. and Chen, Q.X.: Quaternary transgressions, eustatic changes and shifting of shoreline in east
446 China. *Marine Geology & Quaternary Geology*, 5(4), 69–80. DOI: 10.16562/j.cnki.0256-
447 1492.1985.04.011, 1985 (in Chinese with English abstract).
- 448 Zhang, Y.C., Hu, J.J. and Liu, C.F.: Preliminary recognition of sea and land changes along the east coast of
449 China since the terminal Pleistocene. *Bulletin of the Chinese Academy of Geological Sciences*, 19, 37–52.
450 <https://www.ixueshu.com/document/8e1a59a8c6fd86ca318947a18e7f9386.html>, 1989 (in Chinese with
451 English abstract).
- 452 Zhao, S.L., Yang, G.F., Cang, S.X., Zhang, H.C., Huang, Q.F., Xia, D.X., Wang, Y.J., Liu, F.S., Liu, C.F.:
453 On the marine stratigraphy and coastlines of the western coast of the gulf of Bohai. *Oceanologia Et*
454 *Limnologia Sinica*, 9(1), 15–25
455 http://qdhs.ijournal.cn/hyyhz/ch/reader/create_pdf.aspx?file_no=19780102&flag=&journal_id=hyyhz&year_id=1978, 1978 (in Chinese with English abstract).
- 457 Zhao, X.T., Geng, X.S., Zhang, J.W.: Sea level changes of the eastern China during the past 20000 years.
458 *Acta Oceanologia Sinica*, 1(2), 269–281.

-
- 459 http://www.hyxb.org.cn/aos/ch/reader/create_pdf.aspx?file_no=19790208&year_id=1979&quarter_id=2&f
460 alg=1, 1979.
- 461 Zong, Y.: Mid-Holocene sea-level highstand along the southeast coast of China. *Quaternary International*,
462 117, 55–67. DOI: 10.1016/S1040-6128(03)00116-2, 2004.

Table 1. Analytical data used to establish SLIPs.

Beta-lab code	Depth (m)	Altitude (m, msl)	Dated material	$\delta^{13}\text{C}$ (‰)	Conventional age (BP)	Calibrated age (BP) (2σ)	Median age (BP)	Indicative meaning and range	Sediment compaction (m)*	Palaeo-mean sea level
Core DC01										
329636	8.40	-4.66	Peat	-26.8	6950±40	7523-7430	7487	Terrestrial peat		
329637	9.27	-5.53	Bulk organic	-18.2	7410±60	8372-8153	8248	Terrestrial peat		
Core QX01										
329647	5.52	+0.36	Bulk organic	-22.5	4300±30	4892-4829	4343**	1.78±0.53	0.29±0.04	-1.14±0.57
329644	6.35	-1.19	Bulk organic	-23.6	5010±50	5900-5644	5226**	1.78±0.53	0.30±0.04	-2.68±0.57
329643	7.20	-2.04	Bulk organic	-25.0	5090±30	5912-5748	5288**	1.78±0.53	0.25±0.03	-3.58±0.56
329641	8.20	-3.04	Peat	-24.6	5830±30	6732-6554	6647	1.78±0.53	0.24±0.03	-4.58±0.56
329642	8.70	-3.54	Peat	-24.3	6030±40	6981-6778	6875	1.78±0.53	0.21±0.03	-5.11±0.56
329645	9.16	-4.00	Peat	-27.4	6220±40	7250-7006	7117	1.78±0.53	0.18±0.02	-5.60±0.55
329640	11.39	-6.23	Peat	-25.3	7010±30	7935-7786	7855	1.78±0.53	0.01±0.01	-8.00±0.54
329646	13.05	-7.89	Peat	-25.1	7200±30	8057-7952	8002	Terrestrial peat		
Core QX03										
353792	2.91	1.47	Peat	-20.6	2350±30	2461-2326	2357	Terrestrial peat		
353794	4.90	-0.42	Peat	-24.0	3390±30	3699-3569	3634	1.78±0.53	0.16±0.02	-2.01±0.55
353796	7.39	-3.01	Plant material	NA	5930±30	6799-6671	6752	1.78±0.53	0.10±0.02	-4.68±0.55
353798	8.63	-4.25	Plant material	-26.7	6410±40	7420-7271	7350	1.78±0.53	0.01±0.01	-6.02±0.54
353800	9.60	-5.22	Plant material	-28.2	6690±40	7622-7478	7562	Terrestrial peat		
353802	12.40	-8.02	Plant material	-28.3	7280±40	8429-8325	8397	Terrestrial peat		
Core QX02										

332798	3.65	-0.08	Bulk organic	-23.6	3680±30	4091-3913	3517**	1.78±0.53	0.30±0.04	-1.57±0.57
332792	5.68	-2.11	Bulk organic	-24.0	5450±30	6300-6204	5718**	1.78±0.53	0.36±0.04	-3.54±0.57
333329	7.27	-3.70	Peat	-26.7	6350±30	7331-7240	7283	1.78±0.53	0.32±0.04	-5.16±0.57
333330	8.98	-5.41	Peat	-26.3	6600±30	7522-7434	7494	1.78±0.53	0.19±0.02	-7.00±0.55
333331	10.97	-7.40	Peat	-27.2	7020±30	7934-7792	7867	Terrestrial peat		
333333	12.42	-8.85	Peat	-26.3	7140±40	8023-7925	7966	Terrestrial peat		
Core ZW15										
255821	1.6	0.03	Bulk organic	-22.5	2930±30	3168-2976	2584**	1.78±0.53	0.32±0.04	-1.44±0.57
356208	12.6	-10.97	Plant material	-25.0	7450±40	8358-8186	8271	1.78±0.53	0.00	-12.75±0.53
356209	13.5	-11.87	Plant material	-25.5	7640±40	8521-8381	8430	Terrestrial peat		
Core Q7										
358054	1.3	2.16	Bulk organic	-20.4	530±30	559-510	540	1.78±0.53	0.10±0.02	+0.49±0.55
357153	17.2	-13.74	Plant material	-28.0	7990±40	9005-8705	8868	1.78±0.53	0.16±0.02	-15.36±0.55
357157	18.85	-15.39	Bulk organic	-24.6	9140±40	10411-10226	9718**	1.78±0.53	0.00	-17.18±0.53
Core CZ01										
395014	15.42	-8.53	Peat	-27.5	8930±40	10099-9914	10047	Terrestrial peat		
Core CZ02										
395022	12.19	-6.42	Peat	-23.1	7950±30	8980-8648	8830	Terrestrial peat		
Core CZ03										
395026	4.42	-0.48	Bulk organic	-24.2	2730±30	2877-2762	2325**	1.78±0.53	0.12±0.02	-2.15±0.55
395027	6.15	-2.21	Peat	-25.1	4790±30	5593-5470	5517	1.78±0.53	0.19±0.02	-3.80±0.55
395028	6.54	-2.57	Bulk organic	-27.1	5830±30	6732-6554	6114**	1.78±0.53	0.18±0.03	-4.18±0.56
395029	7.51	-3.54	Peat	-26.7	6230±30	7251-7019	7167	1.78±0.53	0.14±0.02	-5.19±0.55
395030	9.22	-5.25	Peat	-27.3	6640±30	7576-7468	7528	1.78±0.53	0.01±0.01	-7.03±0.54

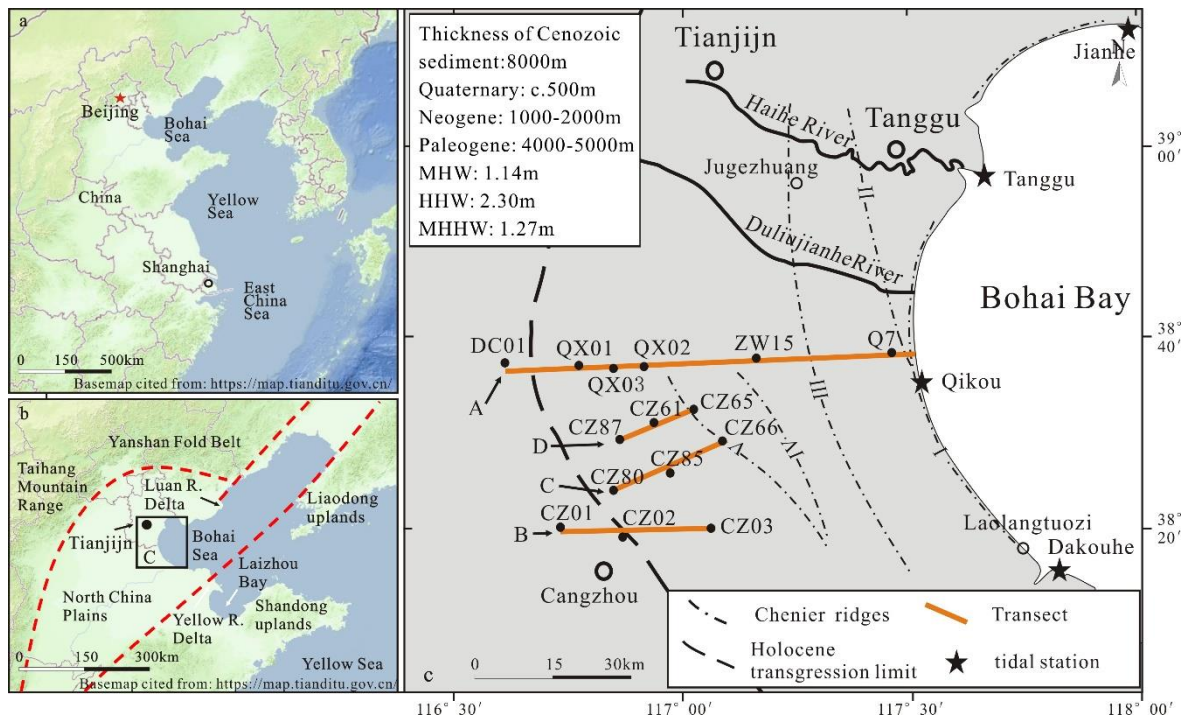
395031	9.34	-5.37	Peat	-20.0	6660±30	7583-7483	7535	1.78±0.53	0.00	-7.15±0.53
395032	10.23	-6.26	Peat	-27.2	6900±30	7794-7669	7726	Terrestrial peat		
395034	12.4	-8.43	Peat	-27.2	7290±30	8171-8025	8102	Terrestrial peat		
Core CZ87										
403413	2.66	1.8	Bulk organic	-20.8	2420±30	2696-2351	2446	Terrestrial peat		
403414	4.51	-0.05	Bulk organic	-23.8	3330±30	3637-3477	3566	Terrestrial peat		
406826	5.75	-1.29	Bulk organic	-24.1	4020±30	4536-4420	3970**	1.78±0.53	0.25±0.03	-2.83±0.56
403417	11.05	-6.59	Plant material	-27.9	6300±30	7275-7165	7223	1.78±0.53	0.04±0.01	-8.33±0.54
403418	12.62	-8.16	Plant material	-27.6	6990±30	7876-7736	7829	Terrestrial peat		
Core CZ61										
407339	2.52	1.24	Bulk organic	-20.8	2310±30	2359-2306	2337	Terrestrial peat		
406823	4.72	-0.96	Plant material	NA	2780±30	2952-2793	2877	1.78±0.53	0.16±0.02	-2.58±0.55
406824	6.20	-2.44	Bulk organic	-23.9	6100±30	7029-6884	6433**	1.78±0.53	0.25±0.03	-3.98±0.56
403397	9.73	-5.97	Plant material	-19.6	6760±30	7664-7577	7615	1.78±0.53	0.00	-7.75±0.53
403398	11.04	-7.37	Plant material	-27.5	7000±30	7932-7756	7842	Terrestrial peat		
403399	12.90	-9.14	Plant material	-28.0	7160±30	8018-7939	7980	Terrestrial peat		
Core CZ65										
399705	4.93	-1.97	Bulk organic	-18.5	3920±30	4428-4280	3397	Terrestrial peat		
399708	9.58	-6.62	Plant material	-27.2	7000±30	7883-7756	7823	1.78±0.53	0.01±0.01	-8.39±0.54
399710	11.50	-8.54	Plant material	-27.1	7250±30	8162-8001	8080	Terrestrial peat		
Core CZ80										
403401	3.73	2.69	Bulk organic	-20.3	3170±30	3452-3346	3400	Terrestrial peat		
403403	6.57	-0.15	Bulk organic	-22.1	5050±30	5901-5726	5298	1.78±0.53	0.20±0.03	-1.74±0.56
406825	8.75	-2.33	Peat	NA	5840±30	6736-6562	6660	1.78±0.53	0.09±0.01	-4.02±0.54

403408	11.53	-5.11	Plant material	-27.5	6450±30	7428-7313	7370	Terrestrial peat		
403409	12.05	-5.63	Plant material	-27.9	6610±30	7565-7440	7503	Terrestrial peat		
403410	12.34	-5.92	Plant material	-26.4	6860±30	7759-7618	7687	Terrestrial peat		
403411	13.84	-7.42	Plant material	-24.6	7300±30	8175-8029	8105	Terrestrial peat		
Core CZ85										
399719	3.67	0.94	Bulk organic	-20.5	3460±30	3671-3641	3225**	1.78±0.53	0.17±0.03	-0.68±0.56
399720	6.77	-2.16	Bulk organic	-25.4	5830±30	6732-6554	6114**	1.78±0.53	0.08±0.01	-3.87±0.54
399721	8.33	-3.72	Plant material	-26.4	6020±30	6947-6785	6862	1.78±0.53	0.01±0.01	-5.49±0.54
399722	12.70	-8.09	Plant material	-28.0	7270±30	8165-8015	8096	Terrestrial peat		
Core CZ66										
399712	3.62	0.25	Bulk organic	-23.4	3930±30	4440-4282	3856**	1.78±0.53	0.32±0.04	-1.22±0.57
399713	5.21	-1.34	Bulk organic	-25.1	5730±30	6632-6445	5992**	1.78±0.53	0.39±0.05	-2.74±0.58
399714	8.14	-4.27	Plant material	-27.4	6710±30	7651-7510	7581	1.78±0.53	0.24±0.03	-5.81±0.56
399715	10.03	-6.16	Plant material	-26.6	6790±30	7675-7587	7635	1.78±0.53	0.08±0.01	-7.86±0.54
399716	12.49	-8.62	Plant material	-27.1	7220±30	8156-7965	8021	Terrestrial peat		
399718	13.63	-9.76	Plant material	-27.6	7670±30	8523-8406	8452	Terrestrial peat		

464 s* Sediment compaction = 10% of compressible thickness divided by lapse time of deposition in the past 9000 years

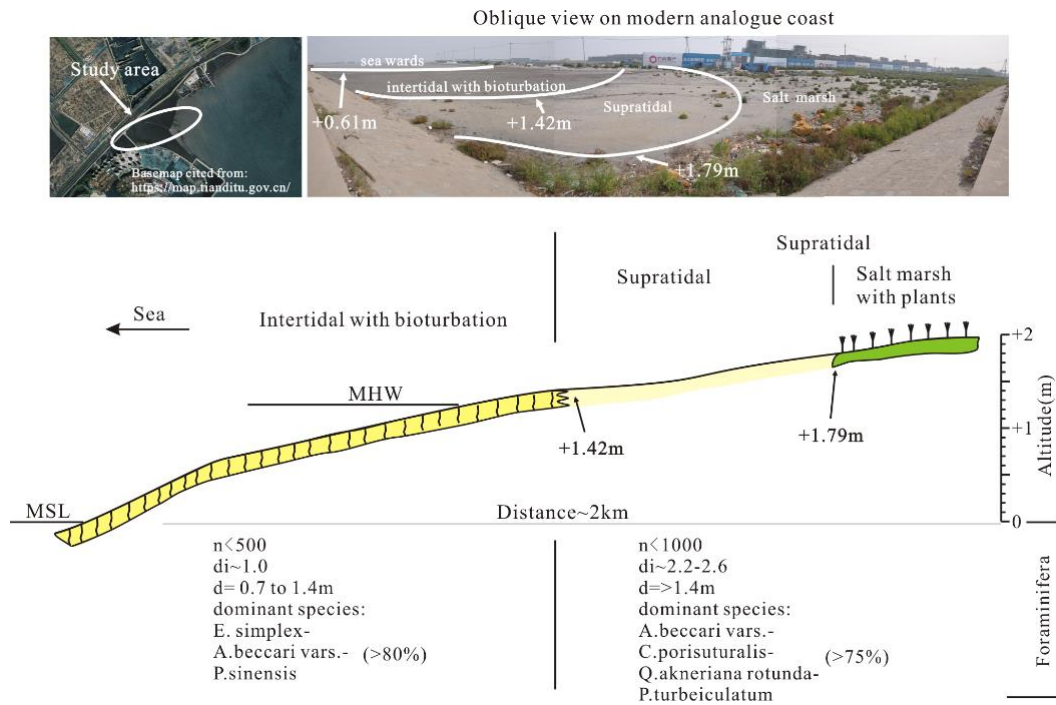
465 ** corrected for marine influence on salt marsh organic sample fraction ages of peaty clay

466

467 **Figure captions**

468

469 **Figure 1. The study area; (a) location of Bohai Bay and Yellow Sea; (b) location of the study area and major river**470 **deltas; red dashed lines indicate the topographic boundaries of coastal lowland, (c) locations of boreholes,**471 **transects A, B, C, D, Chenier ridges (Su et al. (2011; Wang et al., 2011) and Holocene transgression limit (Xue,**472 **1993). The basemap of Fig.1a and Fig.1b are cited from "map world" (<https://www.tianditu.gov.cn/>, National**473 **Platform for Common Geispatial Information Services, China)**

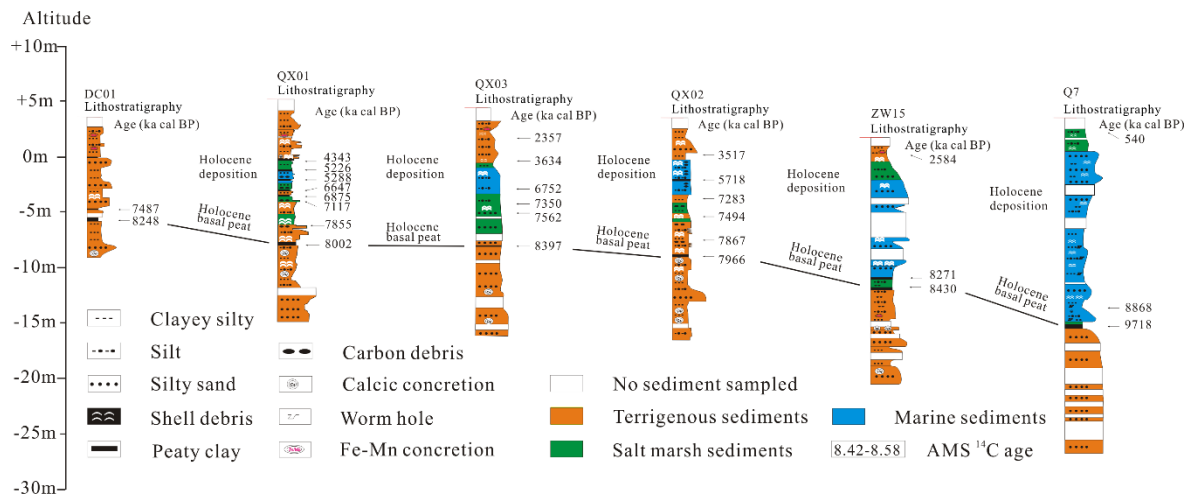


474

475 **Figure 2. Schematic cross-section of the modern tidal flat of the study area showing two characteristic**

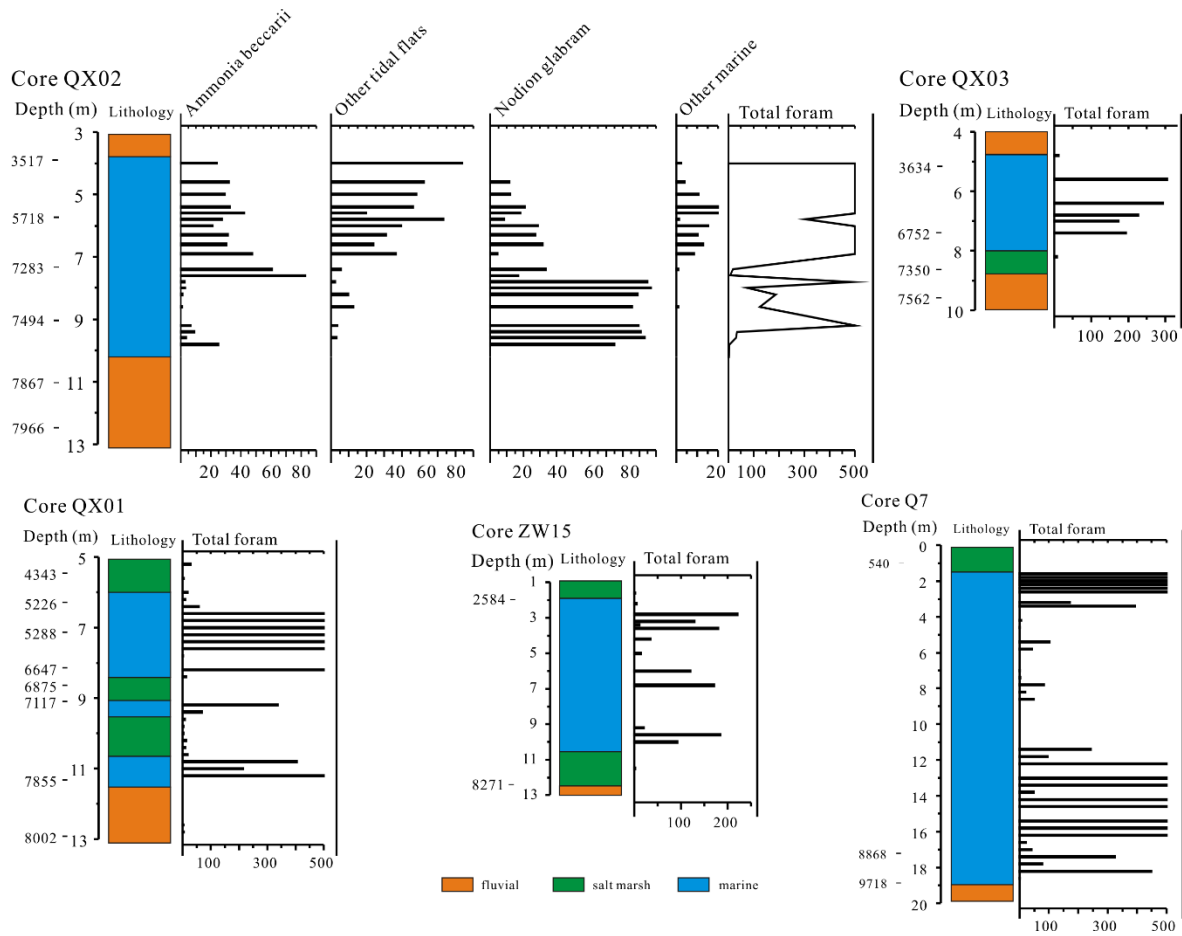
476 **foraminiferal zones. The basemap of study area is derived from "map world" (<https://www.tianditu.gov.cn/>,**

477 **National Platform for Common Geospatial Information Services, China)**



478

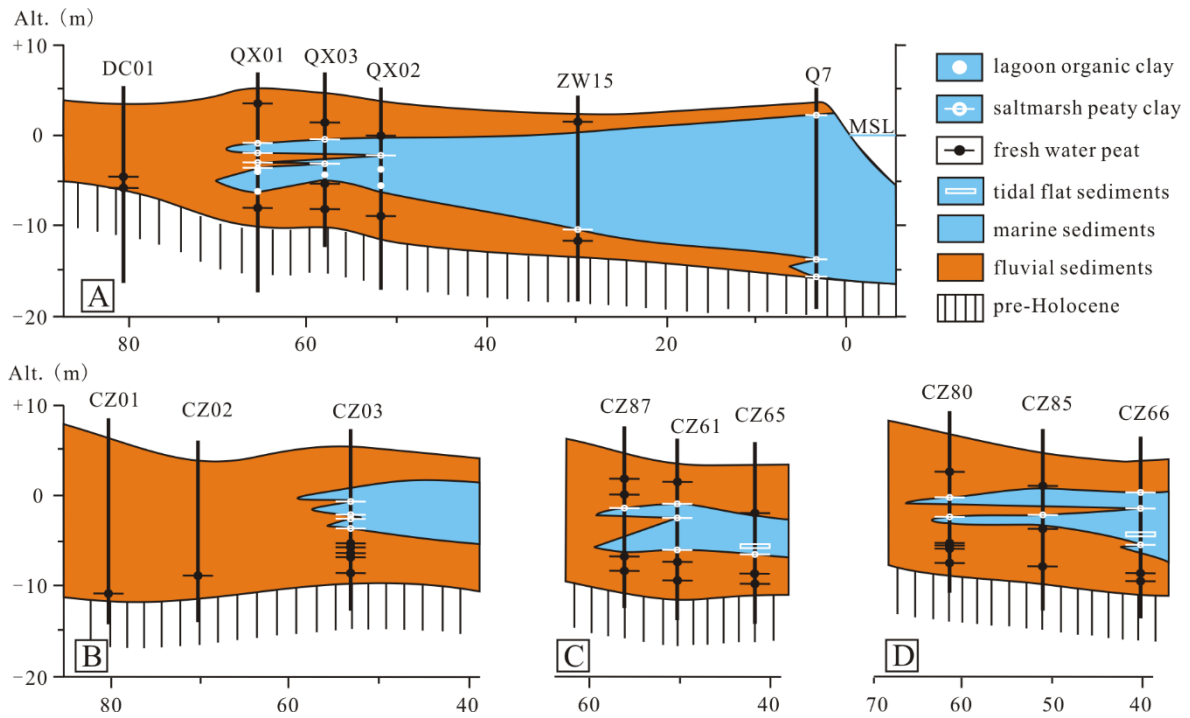
479 **Figure 3. The lithostratigraphy of transect A, with details of dated sedimentary horizons.**



480

481

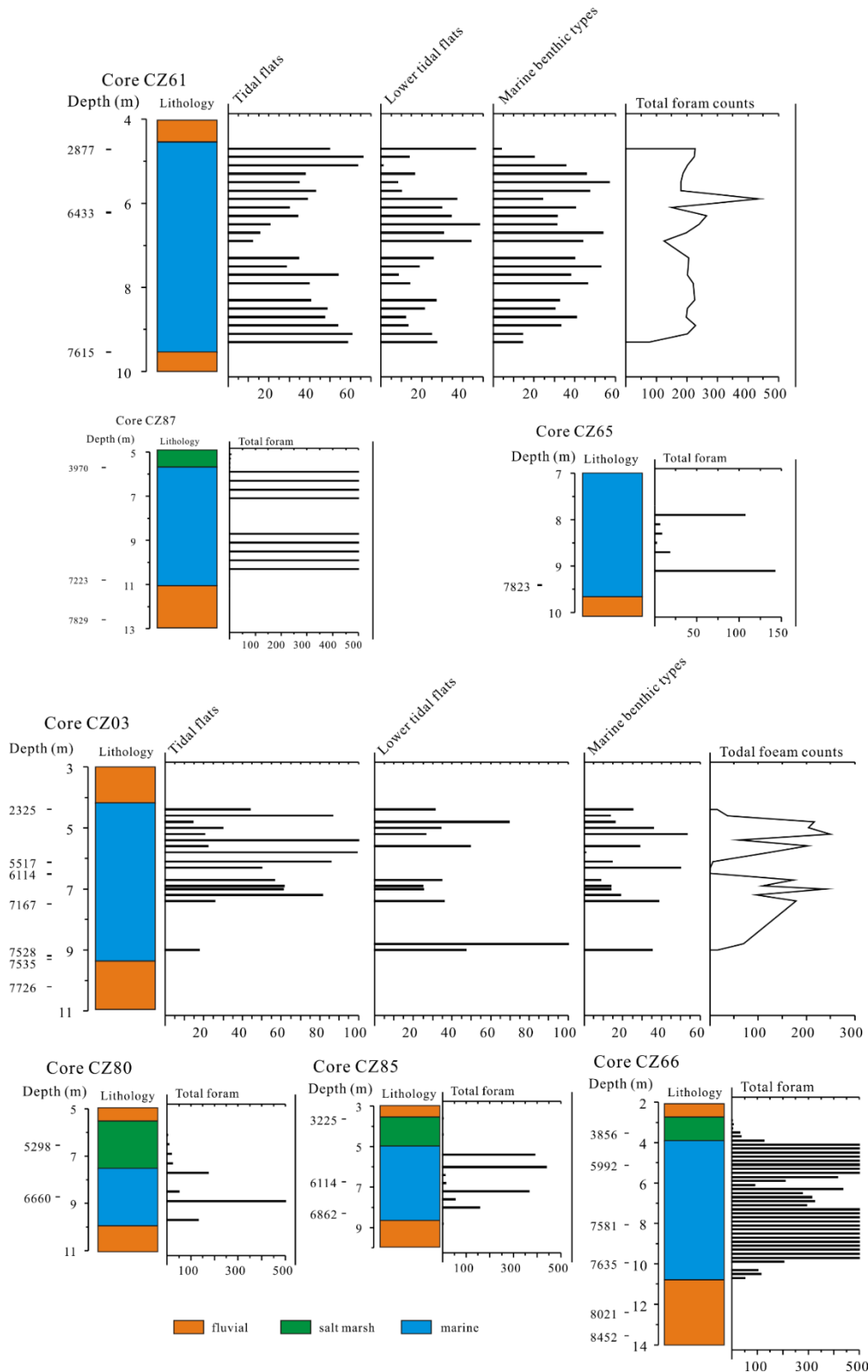
Figure 4. Foraminiferal counts from five cores of transect A. Counts > 500 are shown as 500.



482

483

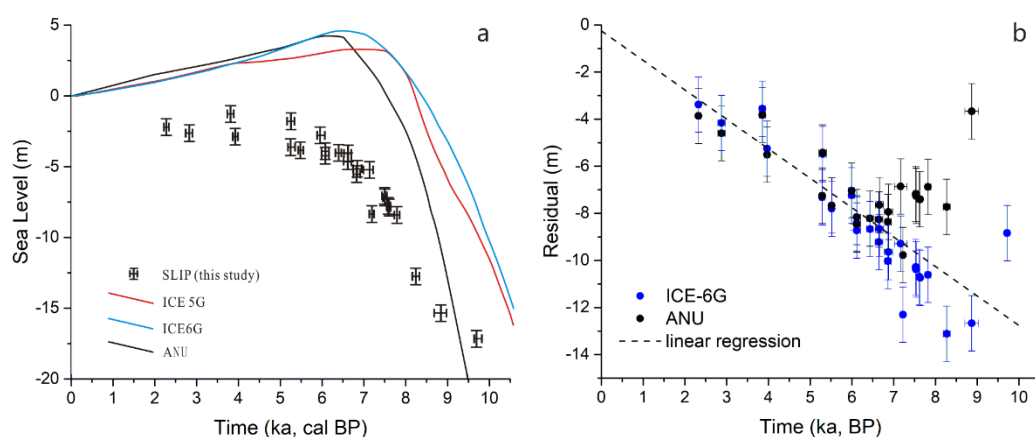
Figure 5. The lithostratigraphy of transects B, C and D, with details of dated sedimentary horizons.



484

485 **Figure 6. Foraminiferal counts from five cores of transects B, C and D. Counts > 500 foraminifera are shown as**

486 **500.**



487

488 **Figure 7. Observed and predicted sea level in Bohai Bay and resulting residuals; (a) SLIPs generated in this study**489 **and sea-level predictions. ICE-5G, ICE-6G and ANU are GIA models described in section 3.6. Lithospheric**490 **thickness (km): 65 (ANU), 90 (5G and 6G); upper mantle viscosity (Pa s) = 0.5×10^{21} (ANU, 5G, 6G); lower mantle**491 **viscosity (Pa s): 10×10^{21} (ANU), 2.7×10^{21} (5G), 3.2×10^{21} (6G); see also Table S1; age error bars are too small to be**492 **clearly visible. (b) Sea-level residuals plotted against time. Residuals are the difference between SLIPs and**493 **interpolated model data points. Error bars are derived from SLIP uncertainties. The trend line (dashed line) is**494 **computed as a least-squares regression on the mean residuals obtained with ANU and ICE-6G. The regression line**495 **approximates zero elevation remarkably closely which gives confidence that the calculated 1.25 mm/a for the non-**496 **GIA component is correct.**

497

498 Author contribution

Author name	Contributions
Fu Wang	Scientific questions choice, design of field work including sampling and measurements, data analyses, results and discussion, paper writing and revising.
Yongqiang Zong	Revise part of the paper and English writing check.
Barbara Mauz	Revise part of the paper and English writing check.
Jianfen Li	Sampling and foraminifera analysis.
Jing Fang	Sampling and foraminifera analysis.
Lizhu Tian	Sampling and foraminifera analysis.
Yongsheng Chen	Sampling and foraminifera analysis.
Zhiwen Shang	Sampling and foraminifera analysis.
Xingyu Jiang	Sampling and foraminifera analysis.
Giorgio Spada	GIA model work and writing sec 3.6
Daniele Melini	GIA model work and residual calculation

499